Research Square

Preprints are preliminary reports that have not undergone peer review.
They should not be considered conclusive, used to inform clinical practice,
or referenced by the media as validated information.

Event-dependent flash-flood regulation by small reservoirs in the Qianhe River Basin: A BTOP-based scenario analysis

Zehua Lu
Sichuan University
Ming Li
Sichuan University
Tianqi Ao
aotianqi@scu.edu.cn
Sichuan University
Liwen Xing
Sichuan University

Article

Keywords: small-reservoir groups, BTOP-DRN, distributed reservoir nodes, flash-flood simulation, reservoir-state uncertainty

Posted Date: November 3rd, 2026

DOI: https://doi.org/10.21203/rs.3.rs-11362834/v1

License: This work is licensed under a Creative Commons Attribution 4.0 International License.
Read Full License

Additional Declarations: No competing interests reported.

Event-dependent flash-flood regulation by small reservoirs in the Qianhe River Basin: A BTOP-based scenario analysis

Zehua Lu[a,b], Ming Li[a], Tianqi Ao[a,*], Liwen Xing[a,*]

a. State Key Laboratory of Hydraulics and Mountain River Engineering, College of Water Resource & Hydropower, Sichuan University, Chengdu, China 610065;

b. Sichuan Provincial Department of Water Resources, Chengdu, China 610065

* Corresponding Author: Tianqi Ao State Key Laboratory of Hydraulics and Mountain River Engineering, College of Water Resource & Hydropower, Sichuan University, Chengdu, China 610065

Email address: aotianqi@scu.edu.cn.

* Corresponding Author: Liwen Xing State Key Laboratory of Hydraulics and Mountain River Engineering, College of Water Resource & Hydropower, Sichuan University, Chengdu, China 610065

Email address: stwen028@gmail.com.

Abstract:

Spatially dispersed small reservoirs can alter flash-flood routing, but their event-scale effects are difficult to constrain without operational records. We coupled tributary storage-release nodes to BTOP routing in the Qianhe River Basin, representing 15 small reservoirs as nine equivalent nodes. The underlying BTOP model was calibrated with 12 hourly storm-flood events and independently evaluated against six further events. Validation Nash-Sutcliffe efficiency values ranged from 0.74 to 0.87, with a mean of 0.81. Five prescribed reservoir-state scenarios varied initial storage and the spill threshold. Under the reference scenario, simulated outlet peak attenuation ranged from 0 to 2.04% and averaged 1.27%; event-volume reduction averaged 0.14%, and peak timing changed by at most 1 h. Mean event-level peak-attenuation ranges were 0.91 and 0.96 percentage points over the tested initial-storage and spill-threshold intervals, respectively. These ranges describe conditional scenario responses and do not rank intrinsic parameter importance. The contribution is a tributary-based implementation

for examining small regulation signals under limited operating data. The results are restricted to the six events and prescribed states; they neither reconstruct historical reservoir operation nor establish an advantage over an outlet-aggregated reservoir representation.

Keywords: small-reservoir groups; BTOP-DRN; distributed reservoir nodes; flash-flood simulation; reservoir-state uncertainty

1. Introduction

Flash floods develop rapidly and can be highly destructive in small and medium-sized mountainous basins. Their severity reflects interactions among extreme rainfall, steep topography, soil and land-surface properties, and hydraulic infrastructure. Short-duration precipitation extremes are particularly sensitive to climate warming and may intensify further, increasing flash-flood risk in small basins[1,2]. Mountain catchments have steep gradients, short flow paths and rapid runoff concentration, producing hydrographs with sharp rising and recession limbs[3]. These dynamics make simulations sensitive to rainfall observations, model time step and antecedent hydrological conditions. In mountainous regions of China, short warning times and sparse hydrological monitoring further constrain flash-flood prediction[4]. Reliable rainfall-runoff simulation in data-scarce basins is therefore central to early warning and risk management.

Flood modelling has progressed from empirical methods to physically based and distributed hydrological models. TOPMODEL, SWAT and VIC represent complementary controls on runoff generation, catchment water cycling, and land-surface water and energy exchanges[5-7]. In mountainous basins, however, rainfall heterogeneity, topographic control and limited observations create substantial uncertainty in calibration and process representation. The Prediction in Ungauged Basins initiative identified reliable parameter and process estimation under limited observations as a central hydrological challenge[8]. BTOP extends TOPMODEL through topographic-index calculations, block-wise computation and channel routing at grid

scale[9]. Coupling BTOP with Muskingum-Cunge routing has supported runoff simulation in humid and topographically complex basins[10]. Regionalization, hybrid modelling and related developments have further adapted BTOP to mountainous basins in south-western China[11-13].

Reservoirs, ponds and other retention structures can intercept runoff, regulate releases and alter river-network connectivity. Whereas large reservoirs strongly modify river flow regimes, dispersed small reservoirs can exert cumulative effects through local detention and delayed release[14-16]. These effects depend on reservoir density, storage, antecedent state and hydrological connectivity[17,18]. Distributed reservoirs can also change tributary routing and downstream flood-wave superposition, especially when delayed releases coincide with main-channel peaks[19]. Recent models explicitly represent small-reservoir networks[20], but their event-scale influence on flash floods in data-scarce mountain basins remains uncertain. Meteorological forcing can substantially influence flood simulations in small mountainous catchments[21]. Reservoir operation and representation can also modify simulated streamflow responses, depending on storage-release assumptions and reservoir-network characteristics[22-25]. Ignoring these spatial and operational controls may therefore bias estimates of peak magnitude, flood-volume distribution and hydrograph shape.

Distributed small-reservoir models and alternative reservoir-coupling approaches already exist[26]. The present question is therefore how a simplified tributary-based representation changes event-scale BTOP output when reservoir operations are poorly observed. In this setting, hydrological model performance, the numerical effect of adding reservoir storage, and the accuracy of historical reservoir operation are distinct questions. A controlled configuration comparison can address the second question, while operational observations and structural alternatives are needed for the third and for evaluating the value of spatial detail.

We implement a distributed reservoir-node extension of BTOP (BTOP-DRN) for the Qianhe River Basin. The extension adds node storage states, water-limited

background releases and threshold spills to the existing runoff-generation and routing framework. Reservoirs are grouped by tributary, and regulated outflow is routed downstream together with bypass runoff. Across six independent storm-flood events, we ask how large the resulting outlet changes are and how they vary across prescribed initial-storage and spill-threshold scenarios. We evaluate peak attenuation, event-volume redistribution, mean discharge before the reference peak and peak timing. The seven-day antecedent precipitation index describes catchment wetness independently of reservoir storage. The study contributes a basin-specific implementation and a conditional assessment of regulation.

2. Study area, data and baseline model

2.1 Study area

The Qianhe River is a tributary of the Jialing River in the Yangtze River system. It rises in Chengkou County, Chongqing, and flows through Xuanhan County, Sichuan. After joining the Houhe River at Dongjiangkou, it becomes the Zhouhe River and ultimately drains to the Jialing and Yangtze rivers. The study basin spans 107.94-109.00° E and 31.29-31.90° N and has a humid subtropical monsoon climate. The Nanba Hydrological Station controls a drainage area of approximately 2,146.8 km². Mean annual precipitation is 1,000-1,400 mm, concentrated mainly from May to September, and mean annual temperature is 13-18 °C. The steep upper basin lies in the Daba Mountains and contains abundant karst terrain. Valleys widen through the middle reaches, while gentler hills and more sinuous channels characterize the lower basin. Rapid hydrological response and intense short-duration rainfall make the basin susceptible to flash floods, landslides and debris flows[27-29]. Figure 1 shows the study area.

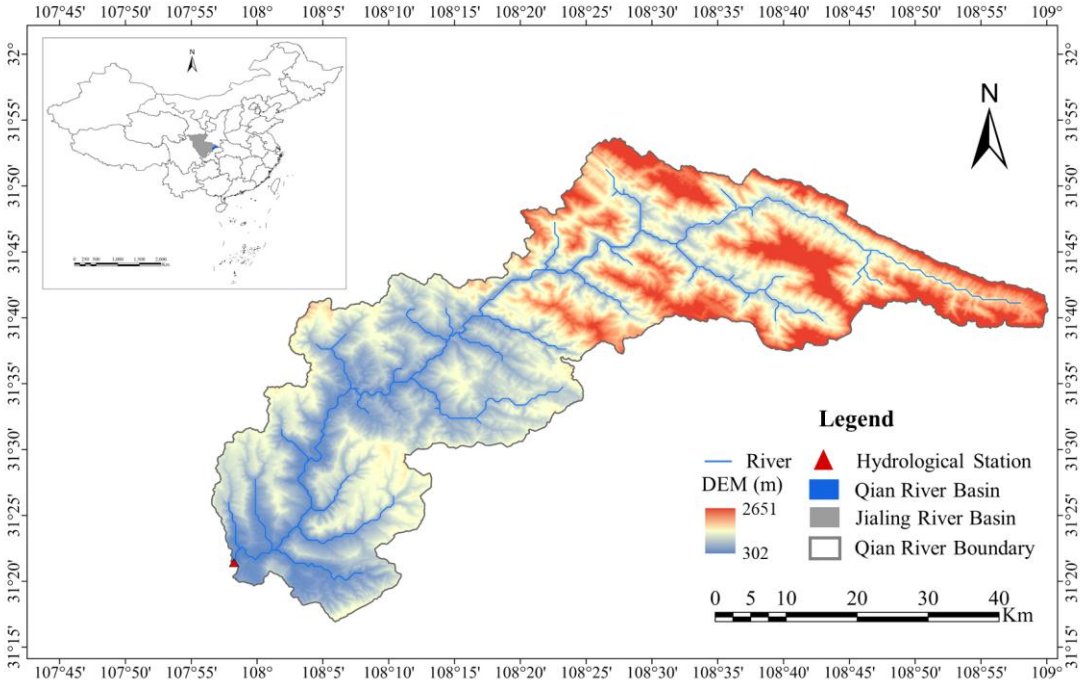


Figure 1. Location and topography of the Qianhe River Basin.

2.2 BTOP model

BTOP is a semi-distributed hydrological model based on the block-wise application of TOPMODEL. of rainfall-runoff, soil-moisture, groundwater and channel-flow processes. Coupling BTOP with Muskingum-Cunge routing yields BTOPMC, the core of the Yamanashi Hydrological Model. Physically interpretable semi-distributed models remain useful in data-scarce mountain basins, but performance should be judged using multiple metrics[30]. The present BTOP implementation has seven calibration parameters. These comprise three global soil parameters (Dclay, Dsand and Dsilt) and four sub-basin parameters (m, SDbar, a and n). Table 1 summarizes their definitions and ranges.

Table 1. Definitions, units, search ranges, and calibrated values of the seven BTOP parameters.

Spatial Partition	Parameter	Physical Meaning	Unit	Range	Calibrated value
Root	a	Drying coefficient	-	-10-10	3.111
Unsaturated/ Saturated	m	Runoff attenuation coefficient	m	0.01-0.1	0.033
Unsaturated	SDbar	Average saturation deficit of the unsaturated layer	m	0.001-0.9	0.227
Channel	n	Block average Manning's coefficient	sm-1/3	0.0001-0.8	0.042
Saturated	Dclay	Coefficients of discharge ability for clay, sand, and silt	mh-1	0.01-2.0	1.108
	Dsand		mh-1	0.01-2.0	0.619
	Dsilt		mh-1	0.01-2.0	0.384

BTOP comprises topographic, runoff-generation and routing modules. The topographic module derives the river network, sub-basins, effective contributing area and topographic index from elevation and soil data. The runoff module represents vegetation, root-zone, unsaturated-zone and groundwater stores at grid scale. We used a Hortonian infiltration-excess runoff scheme. This configuration was retained because the present study focuses on event-scale flash floods generated by short-duration, high-intensity rainfall, for which rapid runoff production associated with infiltration-capacity exceedance can be important. Nevertheless, saturation-excess runoff may also contribute in this humid mountainous basin; therefore, the adopted runoff-generation scheme should be regarded as a structural model assumption rather than a complete representation of all runoff-generation mechanisms. The routing module applies an improved Muskingum-Cunge formulation that accommodates backwater effects and negative flow. Only the channel Manning roughness coefficient requires calibration. The compact, physically interpretable parameter set limits calibration demands while retaining spatial variation in topography, soil and land cover.

2.3 Data

We assembled records from one hydrological station and four rain gauges. Daily runoff and precipitation observations from May 2011 to December 2025 came from the Yangtze River Hydrological Yearbook. A 30-m digital elevation model was obtained from the Geospatial Data Cloud. Land cover followed the International Geosphere-Biosphere Programme classification and a global 30-m land-cover product[31].

Soil texture was derived from the 1-km FAO global soil dataset. Land-cover and soil inputs represented 2020 conditions. Potential evapotranspiration and canopy-top evaporation at 0.1° resolution were obtained from ERA5-Land. All spatial inputs were resampled to 200 m for BTOP calibration. The 200-m grid represents the computational resolution of BTOP and therefore inevitably smooths some fine-scale topographic variability relative to the original 30-m DEM. Small reservoirs were not represented as 200-m reservoir raster cells; instead, their observed locations and storage attributes

were retained and subsequently linked to the corresponding BTOP river-network nodes. The Nanba Hydrological Station defined the basin outlet. Small-reservoir locations and attributes came from Science DataBank (https://www.scidb.cn/s/zqIFVr). Table 2 lists all datasets and their uses.

Table 2. Data sources, resolutions and uses.

Data type	Temporal/Spatial scale	Data form	Data source	Use
Hourly Precipitation	Hourly	Station data	Yangtze River Hydrological Yearbook	Calibration and validation of event-scale BTOP simulations
Hourly discharge	Hourly	Station data	Yangtze River Hydrological Yearbook	Calibration and independent validation
Long-term hydrometeorological data	Daily	Station data	Yangtze River Hydrological Yearbook	Continuous simulation for antecedent states and low-flow characterization
DEM	30 m	Raster	Geospatial Data Cloud	River network extraction and topographic index calculation
Land use	2020	Raster	IGBP classification data	Underlying surface parameters
Soil	1 km	Raster	FAO	Soil parameters
Evapotranspiration	0.1°	Raster	ERA5-Land	BTOP input
Small reservoirs	-	-	Science Data Bank	Construction of regulation nodes

3. Modelling methods

3.1 Modelling framework

The workflow separates BTOP calibration and validation from the reservoir-state scenario comparisons (Figure 2). Twelve hourly events were used for calibration and six for independent validation, after which the BTOP parameters were held fixed. Continuous simulations supplied antecedent catchment states and reference low-flow information. Reservoir attributes and network topology defined nine equivalent nodes from 15 reservoirs. Each of the six events was simulated with the BTOP reference configuration and five BTOP-DRN scenarios. Paired differences quantify peak attenuation, event-volume redistribution, pre-peak mean-flow change and peak timing under identical forcing and catchment parameters.

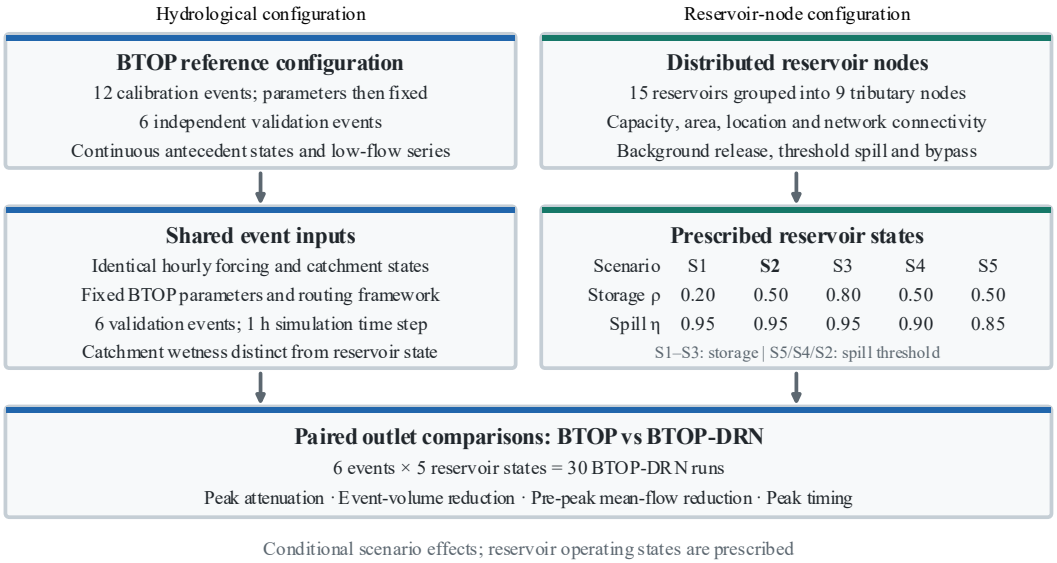


Figure 2. Implemented workflow. BTOP calibration and independent validation precede paired comparisons with nine reservoir nodes under shared event inputs. Five prescribed storage and spill settings are applied to six events, giving 30 BTOP-DRN runs.

3.2 Storm events, calibration-validation design and input data

We screened hourly storm-flood events from the available hydrometeorological record. Events with comparatively large observed peaks at Nanba were prioritized because the analysis targets hydrologically consequential flash floods. Each selected event also contained continuous rainfall and discharge observations across the rising limb, peak and recession. The resulting sample therefore represents large, well-observed events rather than a random sample of all historical floods.

Eighteen events met these criteria. Twelve events calibrated the seven BTOP parameters, and six events were reserved for independent validation. The validation events were 150625, 210829, 210919, 230528, 240711 and 250929, identified using the YYMMDD date format. We optimized parameters against hourly rainfall and discharge using the shuffled complex evolution algorithm (SCE-UA). Search ranges followed Table 1. The population contained six complexes, 15 points per complex and eight points per sub-complex. Optimization stopped after 10,000 evaluations or when objective-function change fell below 1.0×10^{-5}% for six consecutive shuffling loops.

After calibration, the parameter set was transferred unchanged to the six validation events. None of these events contributed to parameter estimation. The same events were

then used to assess scenario-based reservoir regulation. A continuous BTOP simulation provided the catchment state immediately preceding each event and reference-simulated low-flow series for node-specific background-release proxies.

Spatial inputs comprised elevation, river network, land cover, soil and the BTOP grid. Reservoir inputs included location, storage capacity, surface area and the associated grid or tributary. All meteorological and discharge series were resolved hourly, and the model time step was 1 h. Reservoir-surface evaporation was omitted because individual events were short and its expected influence was small. Required BTOP evaporation and leaf-area inputs were nevertheless identical between configurations. Thus, simulated differences arose from the explicit reservoir-node module.

3.3 Construction of equivalent BTOP-DRN regulation nodes

The calibrated BTOP configuration without explicit reservoir nodes provides the common reference hydrograph for the paired comparisons. All catchment inputs and parameters are identical when the reservoir-node module is enabled.

Observed outlet discharge used for calibration may already contain effects of existing reservoirs. Consequently, disabling the explicit reservoir module does not reconstruct a uniquely identifiable historical reservoir-free hydrograph. BTOP-DRN instead measures the response to adding a specified storage-release representation to this common reference. Reference inflow from the reservoir-controlled part of each tributary passes through its equivalent node. The regulated outflow is combined with runoff that bypasses the reservoirs and then enters downstream BTOP routing. The controlled contribution must be replaced by its regulated counterpart, rather than added a second time to the unmodified reference flow.

BTOP-DRN retains the existing runoff-generation and channel-routing formulations and adds tributary storage and release. The nine-node representation retains between-tributary differences in location and downstream pathways. Aggregation does not preserve the individual locations, intervening travel times or

operating rules of reservoirs merged within a tributary.

Reservoirs were linked to BTOP flow-direction or river-network grids and assigned to tributaries. A tributary containing one reservoir retained an individual node. Reservoirs on the same tributary were combined into one equivalent node, with capacity obtained by summing the constituent reservoir capacities equ.1:

$$V_j = \sum_{k \in G_j} V_k \tag{1}$$

Where V_j is the equivalent storage capacity of the *j*-th regulation node, V_k is the storage capacity of the *k-th* small reservoir, and G_j is the set of small reservoirs included in the *j-th* regulation node.

Capacity aggregation conserves total nominal storage but is not a proof of dynamic equivalence. It assumes that grouped reservoirs can be approximated by a shared storage-release state at the equivalent location. This reduces the operating information required while omitting within-group cascade routing and differences in initial state. A comparison with individually represented reservoirs is needed to quantify that approximation.

3.4 Regulation-node calculations

The mathematical addition consists of a storage state and a release calculation at each equivalent node. Equ.2-10 define the node update; Equ.11 combines regulated release with bypass flow before downstream routing. Catchment runoff-generation parameters are unchanged. The distinction from the reference model is the explicit interception, storage and replacement of the controlled tributary contribution.

Continuous water levels, storage-capacity curves, inflows, outflows and operating records were unavailable for the study reservoirs. Detailed operation could therefore not be reconstructed. As commonly required under such data limitations[32,33], we used a simplified storage-detention rule defined by equivalent capacity and a minimum release. The rule represents temporary tributary detention, spill after the threshold is reached and subsequent downstream routing. It does not represent reservoir-specific operator decisions.

The node follows a two-stage background-release and spill rule. Its spill-control storage is a prescribed fraction of nominal capacity Equ.2:

$$S_{c,j} = \eta V_j \tag{2}$$

The spill-threshold coefficient is 0.95 in the reference scenario and 0.85 or 0.90 in the threshold comparison. Below the threshold, background release is limited by the available water; water remaining above the threshold is spilled within the current time step.

To ensure mass conservation within each equivalent reservoir node, the storage–release process is updated explicitly at each model time step. For reservoir node j, let $S_{j,t}$ denote the storage volume at the beginning of time step t, $Q_{in,j,t}$ denote the inflow routed through the reservoir-controlled part of the tributary, and Δt denote the computational time step. The total water available at the node during the current time step is:

$$A_{j,t} = S_{j,t} + Q_{in,j,t}\Delta t + P_{j,t}F_j \tag{3}$$

In Equ.(3), the rainfall term is precipitation depth accumulated during the current step, in metres, multiplied by reservoir surface area, in square metres; it is a water volume rather than a discharge. The background-release volume and the storage remaining after that release are given by Equ.4-5:

$$V_{min,j,t} = min(Q_{min,j}\Delta t, A_{j,t}) \tag{4}$$

$$S^*_{j,t} = A_{j,t} - V_{min,j,t} \tag{5}$$

The minimum operator in Equ.4 prevents background release from exceeding available water. Any remaining storage above the spill-control threshold is discharged as spill Equ.6:

$$V_{spill,j,t} = max(0, S^*_{j,t} - S_{c,j}) \tag{6}$$

Total regulated discharge is the sum of background-release and spill volumes

269 divided by the time step, while end-of-step storage is the remaining water volume
270 Equ.7-8:

271 $$Q_{out,j,t} = \frac{V_{min,j,t} + V_{spill,j,t}}{\Delta t} \quad (7)$$

272 $$S_{j,t+1} = S^{*}_{j,t} - V_{spill,j,t} \quad (8)$$

273 The resulting time-step water balance is expressed by Equ.9:

274 $$S_{j,t} + Q_{in,j,t}\Delta t + P_{j,t}F_j = S_{j,t+1} + Q_{out,j,t}\Delta t \quad (9)$$

275 With immediate spill above the prescribed threshold, end-of-step storage satisfies
276 Equ.10:

277 $$0 \le S_{j,t} \le S_{c,j} = \eta V_j < V_j \quad (10)$$

278 Unregulated bypass flow is added to regulated node discharge, and the combined
279 tributary flow enters downstream BTOP routing Equ.11:

280 $$Q_{DRN,j,t} = Q_{bypass,j,t} + Q_{out,j,t} \quad (11)$$

281 Where $Q_{bypass,j,t}$ represents the runoff contribution that is not intercepted by the
282 equivalent reservoir node.

283 Background release was specified from daily discharge series produced by
284 continuous reference BTOP simulations. A flow-duration curve was constructed for
285 each node, and its 90% exceedance discharge was used as the fixed minimum-release
286 proxy Equ.12. This is a modelling assumption based on simulated low flows, not a
287 measured release schedule or an independently established ecological flow
288 requirement:

289 $$Q_{\min,j} = Q_{90,j} \quad (12)$$

290 The 90% exceedance discharge is equalled or exceeded on 90% of days in the
291 reference series. Node-specific values were held constant across events and scenarios,
292 so changes in the prescribed release did not enter the initial-storage or spill-threshold
293 comparisons. The influence of this release assumption requires separate evaluation.

3.5 Antecedent wetness and initial reservoir-state scenarios

Actual pre-event storage could not be determined because reservoir levels, releases and operating records were unavailable. Storage also reflects withdrawals, managed releases, evaporation, seepage and seasonal practice, not antecedent rainfall alone. We therefore treated initial storage as an uncertain scenario variable. The antecedent precipitation index describes relative catchment wetness but is not interpreted as an observation or inversion of reservoir storage.

3.5.1 Antecedent wetness

For flood event e and rain gauge s, rainfall during the 168 h preceding the onset of the storm is first divided into seven consecutive 24 h periods, and the index is calculated as follows:

$$API_{s,e} = \sum_{d=1}^{7} k^{d-1} P_{s,e,d} \tag{13}$$

Here, the rainfall term denotes cumulative precipitation during each preceding 24 h period; day 1 is closest to storm onset. The baseline daily decay coefficient is 0.85. Equ.13 therefore places the greatest weight on recent rainfall.

Because the gauge network does not resolve antecedent rainfall at each reservoir, gauge indices were combined using the same spatial weights as basin-average rainfall Equ.14:

$$API_e = \sum_{s=1}^{4} w_s API_{s,es} \tag{14}$$

Spatial weights for Tuhuang, Hekou, Liaozi Tianchi and Liaozi Xuetuo were 0.48, 0.21, 0.15 and 0.16, respectively.

The resulting API describes relative antecedent wetness among events. It was not used to assign reservoir storage or to infer a rainfall-storage relationship.

We tested API sensitivity using daily decay coefficients of 0.80, 0.85 and 0.90. API increased with the coefficient, but event rankings remained stable. Rankings were identical at 0.80 and 0.85; at 0.90, only events 240711 and 210919 exchanged adjacent

positions. Spearman correlations among rankings ranged from 0.943 to 1.000. The decay coefficient therefore affected absolute API values more than relative wetness classification.

Table 3. Antecedent precipitation index values for six events under alternative decay coefficients.

k	150625	250929	230528	240711	210919	210829
0.80	12.9	32.8	36.1	44.6	51.1	58.2
0.85	15.9	35.0	37.8	51.0	53.1	65.2
0.90	19.6	37.4	39.6	58.5	55.2	73.3
ΔAPI (%)	51.9%	14.0%	9.7%	31.2%	8.0%	25.9%

3.5.2 Initial storage scenarios

Initial storage was specified as a fraction of node capacity Equ.15:

$$S_{j,0}^{q} = \rho_q V_j \tag{15}$$

where V_j is the equivalent total storage capacity of node j, m^3; $S_{j,0}^{(q)}$ is the initial storage volume under the corresponding scenario, m^3.

Three prescribed initial-storage ratios, 0.20, 0.50 and 0.80, represent low, medium and high states (Table 4). They are exploratory boundary conditions, not measured storage ratios for the historical events.

The difference between spill-control storage and initial storage defines effective available storage before spilling Equ.16:

$$C_{j,0}^{q} = \left(\eta - \rho_q\right) V_j \tag{16}$$

At the reference spill threshold of 0.95, the three initial states leave 0.75, 0.45 and 0.15 times node capacity available before spilling. These differences explain the storage contrast imposed by the design; they do not by themselves establish the resulting outlet response.

Within each scenario, the same initial storage ratio was assigned to every node, while capacities remained node specific. Settings were identical across events and were not adjusted to improve outlet fit. The five settings sample prescribed states and do not exhaust the plausible range of historical reservoir conditions.

3.5.3 Sensitivity to spill threshold and initial storage

A one-factor-at-a-time design compares initial storage at a fixed spill threshold

and the spill threshold at a fixed initial storage. Scenario S2 combines an initial storage ratio of 0.50 with a spill threshold of 0.95. For the first comparison, S1, S2 and S3 use initial storage ratios of 0.20, 0.50 and 0.80. For the second, S5, S4 and S2 use spill thresholds of 0.85, 0.90 and 0.95. Table 4 lists the five unique combinations.

Rainfall, BTOP parameters, antecedent catchment states, node locations and capacities, bypass configuration, background release and time step were held fixed within each event. The parameter intervals were selected for exploratory scenario analysis and were not inferred as probability distributions from reservoir observations.

Table 4. Reservoir-regulation scenarios and parameter settings.

Scenario	Initial storage ratio	Spill threshold	Scenario characteristics
S1	0.20	0.95	Large initial available storage capacity
S2	0.50	0.95	Reference scenario
S3	0.80	0.95	Small initial available storage capacity
S4	0.50	0.90	Medium storage, relatively low spill threshold
S5	0.50	0.85	Medium storage, low spill threshold

All five scenarios were applied to every event. The BTOP reference configuration has no initial-storage or spill-threshold parameter and provides the common comparison baseline.

The design evaluates conditional responses along two parameter sequences. It does not estimate joint parameter interactions or global sensitivity. Because available storage depends on both initial storage and the spill threshold, the two effects should not be interpreted as independent physical mechanisms.

3.5.4 Metrics of regulation and sensitivity

Regulation metrics compare BTOP-DRN with the BTOP reference under identical forcing, catchment state and BTOP parameters. They describe peak flow, finite-window outflow volume, mean discharge before the reference peak and peak timing. Performance metrics instead compare simulated outlet hydrographs with observed discharge.

(1) Peak-flow attenuation rate

The peak-flow attenuation rate characterizes the influence of the reservoir group on peak discharge at the basin outlet. For flood event e under scenario q, the peak-flow

attenuation rate is defined as:

$$R_{p,e}^{q} = \frac{Q_{p,e}^{BTOP} - Q_{p,e}^{DRN,q}}{Q_{p,e}^{BTOP}} \times 100\% \tag{17}$$

The simulated peak discharges from BTOP and BTOP-DRN are, respectively:

$$Q_{p,e}^{BTOP} = \max_{1 \le t \le T_e} Q_{e,t}^{BTOP} \tag{18}$$

$$Q_{p,e}^{DRN,q} = \max_{1 \le t \le T_e} Q_{e,t}^{DRN,q} \tag{19}$$

The two peak discharges are the maxima of the reference and scenario hydrographs over the same event record, in $m^3\ s^{-1}$. Positive peak attenuation denotes a lower scenario peak, zero denotes an unchanged peak magnitude and a negative value denotes enhancement. A negative value alone does not identify the storage or routing mechanism responsible.

(2) Event flood-volume change rate

The event flood-volume change rate characterizes the effect of reservoir storage and release on outlet flood volume within the finite simulation period. The BTOP-simulated flood volume for flood event e is:

$$W_e^{BTOP} = \sum_{t=1}^{T_e} Q_{e,t}^{BTOP} \Delta t \tag{20}$$

The BTOP-DRN-simulated flood volume under scenario q is:

$$W_e^{DRN,q} = \sum_{t=1}^{T_e} Q_{e,t}^{DRN,q} \Delta t \tag{21}$$

where Δt is the model time step. A 1 h time step is used in this study; when discharge is expressed in m^3 / s Δt = 3600 s.

Accordingly, the event flood-volume change rate $R_{v,e}^{q}$ is defined as:

$$R_{v,e}^{q} = \frac{W_e^{BTOP} - W_e^{DRN,q}}{W_e^{BTOP}} \times 100\% \tag{22}$$

The volumes integrate outlet flow over the same finite simulation window. A positive rate denotes lower scenario outflow volume, whereas a negative rate denotes

higher outflow volume. Differences can reflect changes in stored water and release timing across the window boundaries. They do not establish permanent loss or gain of basin water.

(3) Change in peak timing

The change in peak timing is used to evaluate the effect of reservoir regulation on flood-propagation timing. For flood event *e* under scenario *q*, the change in peak timing is defined as:

$$\Delta T_{p,e}^{q} = T_{p,e}^{DRN,q} - T_{p,e}^{BTOP} \tag{23}$$

where $T_{p,e}^{BTOP}$ and $T_{p,e}^{DRN,q}$ are the simulated times of peak discharge for BTOP and BTOP-DRN scenario *q*, respectively. When $\Delta T_{p,e}^{q} > 0$, reservoir regulation delays the outlet peak; when $\Delta T_{p,e}^{q} < 0$, the simulated peak occurs earlier. For the hourly simulations used in this study, $\Delta T_{p,e}^{q}$ is expressed in h.

(4) Reduction in mean discharge over the pre-peak window

A common pre-peak window runs from the start of the analysed event record (t = 0) to the BTOP reference peak, inclusive. This matches the window used in the exported indicator tables. The start index in the following equations denotes the event-record start, rather than an independently detected onset of hydrograph rise. The same indices are used for BTOP and all reservoir scenarios, so shifts in scenario peak time do not change the comparison window. The number of included hourly samples is:

$$N_{r,e} = T_{p,e}^{BTOP} - t_{r,e} + 1 \tag{24}$$

The reference mean discharge over this pre-peak window is:

$$\bar{Q}_{r,e}^{BTOP} = \frac{1}{N_{r,e}} \sum_{t=t_{r,e}}^{T_{p,e}^{BTOP}} Q_{e,t}^{BTOP} \tag{25}$$

The corresponding scenario mean discharge is:

$$\bar{Q}_{r,e}^{DRN,q} = \frac{1}{N_{r,e}} \sum_{t=t_{r,e}}^{T_{p,e}^{BTOP}} Q_{e,t}^{DRN,q} \tag{26}$$

417 The relative reduction in pre-peak mean discharge is:

418 $$R_{r,e}^{q}=\frac{\bar{Q}_{r,e}^{BTOP}-\bar{Q}_{r,e}^{DRN,q}}{\bar{Q}_{r,e}^{BTOP}}\times 100\% \tag{27}$$

419 Positive values indicate lower mean discharge over this defined window; negative
420 values indicate higher mean discharge. This metric summarizes the pre-peak record and
421 does not isolate a strictly rising hydrograph segment or directly measure the rate of
422 flood rise.

423 (5) Simulation accuracy of the outlet flood hydrograph

424 The Nash-Sutcliffe efficiency coefficient (NSE), relative error of peak discharge
425 (RE_p), and relative error of flood volume (RE_v) are used to evaluate the agreement
426 between the observed outlet hydrograph and simulations from BTOP and the different
427 BTOP-DRN scenarios.

428 The NSE for flood event *e* is calculated as:

429 $$NSE_e=1-\frac{\sum_{t=1}^{T_e}\left(Q_{e,t}^{obs}-Q_{e,t}^{sim}\right)^2}{\sum_{t=1}^{T_e}\left(Q_{e,t}^{obs}-\bar{Q}_{e}^{obs}\right)^2} \tag{28}$$

430 where the mean observed discharge is:

431 $$\bar{Q}_{e}^{obs}=\frac{1}{T_e}\sum_{t=1}^{T_e}Q_{e,t}^{obs} \tag{29}$$

432 where $Q_{e,t}^{obs}$ and $Q_{e,t}^{sim}$ are the observed and simulated discharges, respectively, for
433 flood event *e* at time *t*, and the mean observed discharge is defined by the preceding
434 equation.

435 The relative error of peak discharge is defined as:

436 $$RE_{p,e}=\frac{Q_{p,e}^{sim}-Q_{p,e}^{obs}}{Q_{p,e}^{obs}}\times 100\% \tag{30}$$

437 $$Q_{p,e}^{obs}=\max_{1\le t\le T_e}Q_{e,t}^{obs} \tag{31}$$

438 $$Q_{p,e}^{sim}=\max_{1\le t\le T_e}Q_{e,t}^{sim} \tag{32}$$

The observed and simulated flood volumes for flood event *e* are, respectively:

$$W_e^{obs} = \sum_{t=1}^{T_e} Q_{e,t}^{obs} \Delta t \tag{33}$$

$$W_e^{sim} = \sum_{t=1}^{T_e} Q_{e,t}^{sim} \Delta t \tag{34}$$

The relative error of flood volume is defined as:

$$RE_{v,e} = \frac{W_e^{sim} - W_e^{obs}}{W_e^{obs}} \times 100\% \tag{35}$$

When $RE_{p,e} > 0$ or $RE_{v,e} > 0$, the simulated peak discharge or flood volume, respectively, exceeds the observed value; negative values indicate underestimation. To evaluate error magnitude when comparing models and parameter scenarios, $\left|RE_{p,e}\right|$ and $\left|RE_{v,e}\right|$ are also used to represent the absolute relative errors of peak discharge and flood volume, respectively.

(6) Sensitivity evaluation of parameter scenarios

For each event, scenario ranges are calculated separately for the initial-storage sequence (S1-S3) and spill-threshold sequence (S5, S4 and S2). The same calculation can be applied to peak attenuation, event-volume reduction, pre-peak mean-flow reduction and peak-timing change. For a given metric, the range is:

$$\Delta Y_{e,G} = \max_{q \in G}(Y_e^q) - \min_{q \in G}(Y_e^q) \tag{36}$$

Here, G denotes the selected scenario set: {S1, S2, S3} for initial storage or {S5, S4, S2} for the spill threshold. The range is the largest minus the smallest metric value within that event and set. It measures response over the tested interval, not a normalized sensitivity coefficient, confidence interval or exhaustive uncertainty bound. Differences between ranges cannot by themselves rank parameter importance when the sampled intervals differ.

The sign of peak attenuation is also inspected across scenarios. A sign reversal identifies a change between simulated attenuation and enhancement within the sampled

463 settings, but is not a formal test of statistical significance or an explanation of its cause.
464 Results are reported together with the reference scenario and the tested parameter
465 ranges.

466 **4. Application to the Qianhe River Basin**

467 **4.1 Reservoir distribution and equivalent regulation nodes**

468 The inventory contains 15 reservoirs with capacities of 23,200-640,641 m^3 and
469 surface areas of 4,629.56-95,846.07 m^2. Their total nominal capacity is 2,919,530 m^3.
470 Reservoirs were assigned to BTOP grids and grouped by tributary and flow direction
471 using the procedure in Section 3.3. Multi-reservoir groups were represented at their
472 downstream tributary confluence; ungrouped reservoirs retained individual nodes. The
473 nine equivalent capacities sum to the same inventory total. This grouping retains
474 between-tributary positions but omits within-group routing, so its dynamic adequacy
475 remains an approximation. Tables 5 and 6 provide reservoir and node attributes, and
476 Figure 3 shows the spatial setting.

477 Table 5. Attributes of small reservoirs in the Qianhe River Basin.

ID	County	Storage(m^3)	Area(m^2)	Grid number
1	Kai County	521751	79468.44	124828
2		61000	11203.89	141909
3		105361	18449.18	135612
4		105438	18461.53	156820
5		45500	8570.81	147669
6		30400	5933.35	148264
7		97200	17138.19	145368
8	Xuanhan County	139000	23740.00	155628
9		118000	20444.00	158345
10		69000	12506.00	101938
11		89000	15797.00	105388
12		23200	4629.56	99589
13		363908	57195.75	78502
14		510131	77851.30	79710
15		640641	95846.07	120162

478 Table 6. Equivalent reservoir-node aggregation.

Node ID	Number of reservoirs	Reservoir ID	Equivalent storage capacity V(m^3)	Equivalent BTOP node location	Presence of bypass tributary
NO1	2	8, 9	257000	155056	N
NO2	3	2, 3, 15	807002	142482	N
NO3	1	4	105438	156820	Y
NO4	4	1, 5, 6, 7	694851	145368	N
NO5	1	13	363908	78502	Y
NO6	1	11	89000	105388	Y
NO7	1	10	69000	101938	Y
NO8	1	12	23200	99589	Y

Node ID	Number of reservoirs	Reservoir ID	Equivalent storage capacity V(m^3)	Equivalent BTOP node location	Presence of bypass tributary
NO9	1	14	510131	79710	Y

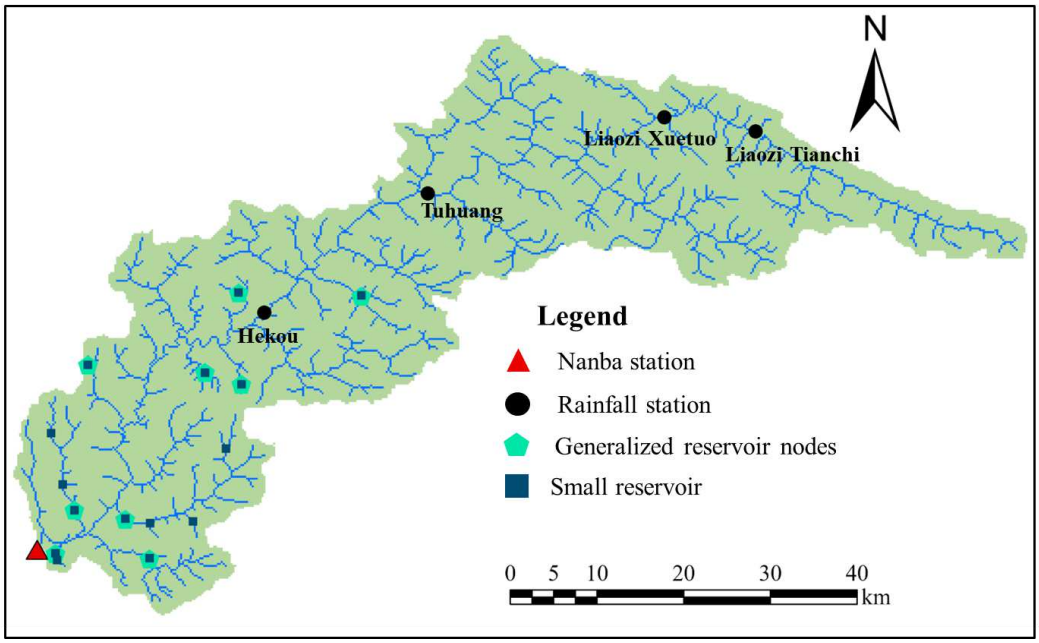


Figure 3. Spatial distribution of equivalent reservoir nodes and the four rain gauges: Tuhuang, Hekou, Liaozi Tianchi and Liaozi Xuetuo. Equivalent-node attributes are listed in Table 6. The Nanba hydrological station defines the basin outlet. Reservoir-node and rain-gauge symbols refer to different network elements.

4.2 Reservoir-regulation scenarios

The five settings in Table 4 were applied to all six validation events, yielding 30 BTOP-DRN runs. Scenario S2 provides the common reference state for event comparisons; the two parameter sequences are defined in Section 3.5.3. Reservoir levels and operating schedules were unavailable, so these runs evaluate prescribed conditions rather than reconstructed operations.

Node geometry, bypass configuration and the node-specific minimum-release proxy from Section 3.4 remained fixed. Meteorological inputs, BTOP parameters and antecedent catchment states were also shared across configurations. API described antecedent catchment wetness and did not determine the initial reservoir storage ratio.

4.3 Results

4.3.1 BTOP calibration and independent validation

A single seven-parameter set was estimated jointly from the 12 calibration events, and the resulting calibrated parameter values are reported in Table 1. The calibrated

model achieved an aggregate NSE of 0.85. After calibration, all seven parameters were fixed and transferred unchanged to the six independent validation events. Figure 4 compares observed and simulated hydrographs, and Table 7 reports event-level metrics.

NSE remained positive for every validation event, ranging from 0.74 to 0.87 with a mean of 0.81. Event 230528 had the highest NSE (0.87), whereas event 240711 had the lowest (0.74). The mean validation NSE was only 0.04 below the calibration value. Thus, the common parameter set retained broadly stable skill when transferred to events excluded from calibration.

Absolute peak-discharge error ranged from 1.91% to 13.97% and averaged 8.06%. Absolute event-volume error ranged from 8.56% to 26.51% and averaged 13.82%. Event 240711 had the smallest peak error, while 230528 had the largest. Event 150625 had the smallest volume error, whereas 210919 had the largest. Strong hydrograph-wide NSE therefore did not guarantee equally small errors in individual flood characteristics.

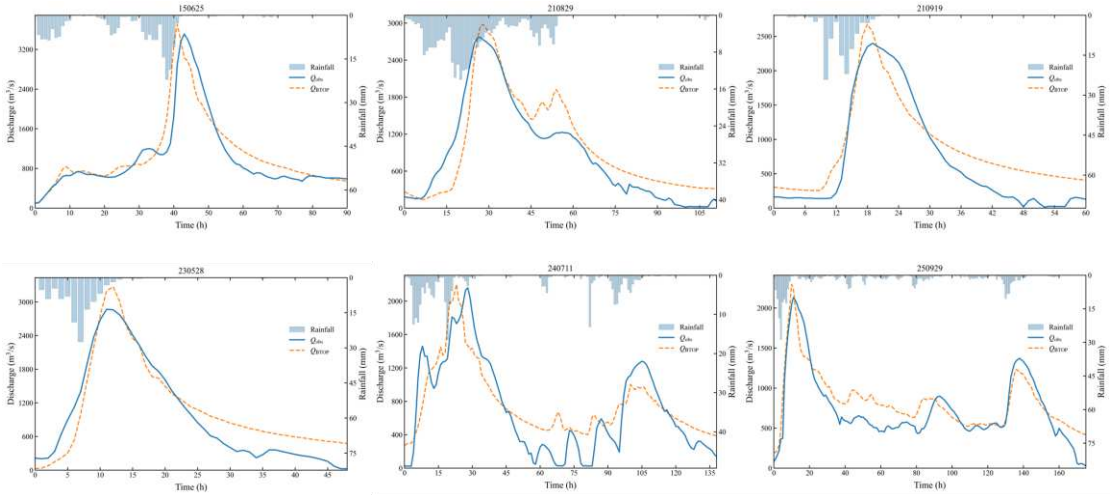


Figure 4. Comparison of observed and BTOP-simulated hydrographs for the six independent validation events. Blue bars denote hourly rainfall plotted on the inverted right-hand axis; the blue solid and orange dashed lines denote observed and simulated discharge, respectively.

Table 7. Performance of the calibrated BTOP model for the six independent validation events.

Event	NSE	RE_p(%)	RE_v(%)
150625	0.83	5.67	8.56
210829	0.82	7.59	12.57
210919	0.84	11.44	26.51
230528	0.87	13.97	13.06
240711	0.74	1.91	9.49
250929	0.77	7.78	12.71
Mean	0.81	8.06	13.82

Note: RE_p and RE_v are reported as absolute relative errors for performance comparison.

4.3.2 Mass-balance closure of the reservoir-node module

The reported water-balance check covers event 230528 under S2. It includes initial and final storage, controlled inflow, direct rainfall on reservoir surfaces and regulated outflow across all nine nodes. This test assesses numerical closure for the specified event and state; it does not validate individual reservoir operations or all scenario runs.

Initial storage totalled 1.4598×10^6 m³. Cumulative inflow and regulated outflow were 26.2008×10^6 m³ and 25.6834×10^6 m³, respectively. Direct rainfall contributed 0.0942×10^6 m³, and final storage was 2.0713×10^6 m³.

The water-balance residual was -1.13 m³, equivalent to a relative closure error of 4.08×10^{-6}%. Maximum instantaneous storage was 2.4843×10^6 m³. This value remained below the spill-control storage (2.7736×10^6 m³) and physical capacity (2.9195×10^6 m³).

Table 8. Water-balance closure and storage-capacity check of the reservoir-node module for event 230528 under scenario S2.

Variable	Value
Total water input	27.7547×10^6 m³
Total water output	27.7547×10^6 m³
Relative closure error	4.08×10^{-6}%
Maximum instantaneous storage	2.4843×10^6 m³
Spill-control storage / total physical storage capacity	$2.7736/2.9195 \times 10^6$ m³

4.3.3 Regulation under the reference scenario

Scenario S2 (ρ = 0.50 and η = 0.95) was adopted as the common reference reservoir-state scenario for event-to-event comparison. The prescribed initial storage ratio and spill-threshold coefficient were not calibrated against observed reservoir operation and therefore should not be interpreted as reconstructions of the actual reservoir states during the historical flood events. To examine whether introducing the conceptual reservoir-node regulation under S2 produced outlet hydrographs that remained consistent with observations, the performance metrics of BTOP and BTOP-DRN under S2 were compared, as summarized in Table 9.

Table 9. Comparison of outlet-hydrograph consistency between BTOP and reference-scenario BTOP-DRN simulations.

Event	NSE_{BTOP}	NSE_{S2}	$RE_{p,BTOP}$ (%)	$RE_{p,\mathrm{S2}}$ (%)	$RE_{v,\mathrm{BTOP}}$ (%)	$RE_{v,\mathrm{S2}}$ (%)
150625	0.83	0.82	5.67	4.39	8.56	8.29
210829	0.82	0.81	7.59	6.22	12.57	12.77
210919	0.84	0.84	11.44	9.37	26.51	26.14
230528	0.87	0.86	13.97	11.65	13.06	12.51
240711	0.74	0.73	1.91	1.91	9.49	9.49
250929	0.77	0.76	7.78	6.41	12.71	12.70
Mean	0.81	0.80	8.06	6.66	13.82	13.65

Note: The BTOP statistics represent independent validation of the calibrated hydrological parameter set. The BTOP-DRN S2 statistics are reported only as an observational consistency check under the assumed reference reservoir state and do not constitute validation of actual reservoir operation. The S2 reservoir-state parameters were not calibrated or selected according to these performance metrics.

Hydrograph performance under S2 remained similar to that under BTOP. Mean NSE changed from 0.81 to 0.80, while mean absolute peak error declined from 8.06% to 6.66%. Mean absolute volume error changed from 13.82% to 13.65%. Peak error declined in five events and was unchanged in event 240711. Thus, the conceptual reservoir module did not materially degrade agreement with observed outlet hydrographs. Because reservoir states were not independently observed, this comparison is a consistency check rather than validation of reservoir operation.

Under reference scenario S2, outlet peak attenuation ranged from 0 to 2.04% and averaged 1.27% across the six events. Five events showed attenuation, with the largest reductions in 230528 (2.04%) and 210919 (1.86%). The other positive responses were 1.20-1.27%. Event 240711 had no difference between its reference and S2 outlet hydrographs. These are differences between model configurations under the prescribed state, rather than observed historical reservoir effects.

Event-volume reduction ranged from −0.18% to 0.49% and averaged 0.14%. Four events had lower scenario outflow volume, event 240711 was unchanged and event 210829 had 0.18% more outflow within the analysed window. The negative value for 210829 therefore denotes an increase in outflow volume. These finite-window differences must be interpreted together with initial and final storage, rather than as permanent water losses.

Reduction in mean discharge over the common event-start-to-reference-peak window ranged from 0 to 2.03% and averaged 0.96%. The largest values occurred in

250929 (2.03%), 230528 (1.77%) and 210919 (1.27%). Figure 5 presents peak, event-volume and pre-peak mean-flow responses with a common event order and separate zero lines.

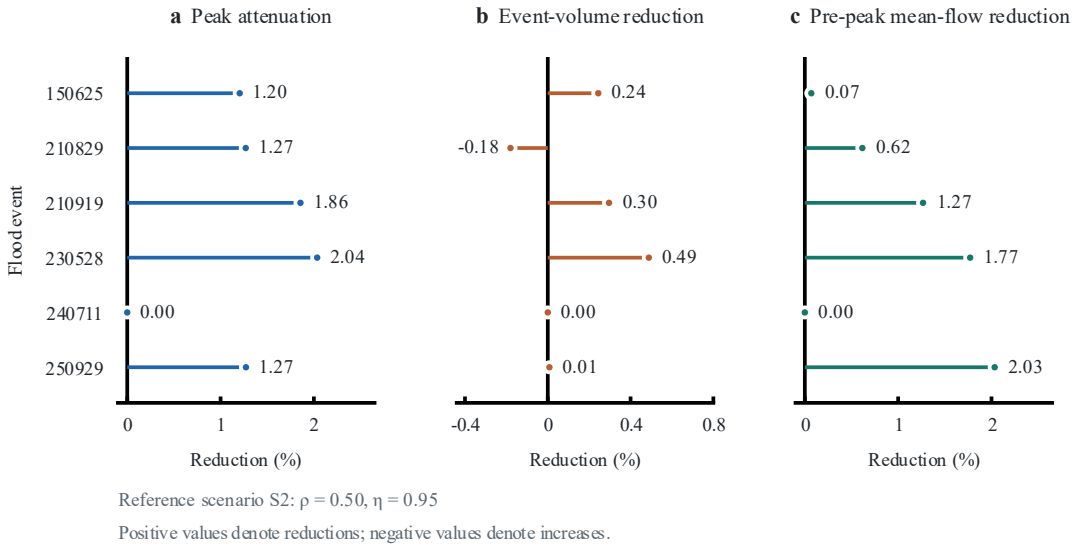


Figure 5. Event-specific outlet responses under S2 (initial storage ratio 0.50; spill threshold 0.95): (a) peak attenuation, (b) relative reduction in event outflow volume and (c) relative reduction in mean discharge from event-record start (t = 0) to the BTOP reference peak, inclusive. Positive values denote reductions relative to BTOP and negative values denote increases. Volume differences refer to the finite simulation window. Independent events are not joined by lines.

The outlet peak occurred 1 h earlier in events 210829 and 230528 and at the same hourly step in the other four events. There was no systematic delay. These one-step differences describe the timing of the sampled maximum; they do not independently establish changes in travel time or tributary-wave synchronization.

4.3.4 Sensitivity to initial reservoir storage

At a fixed spill threshold of 0.95, the ranges of peak attenuation across S1-S3 were 1.19-1.61%, 0-1.27%, 1.86-2.73%, 0.77-2.04%, 0-0.93% and 1.03-1.73%, respectively, in the event order shown in Figure 6a. Each range was less than 1.3 percentage points.

Mean peak attenuation across events was 1.30%, 1.27% and 1.03% at initial storage ratios of 0.20, 0.50 and 0.80, respectively. From the low to high initial state, mean event-volume reduction changed from 0.34% to −0.18%, while mean pre-peak flow reduction changed from 1.44% to −0.67%. Available storage before spilling

declined from 0.75 to 0.15 times node capacity across these prescribed states.

Individual-event responses were not uniformly monotonic. Attenuation decreased with increasing initial storage for 150625 and 250929, while 210829, 210919, 230528 and 240711 showed non-monotonic sequences. For example, event 230528 produced 0.77%, 2.04% and 1.56% attenuation across S1-S3. These outlet values describe the exported scenario results; they do not establish the node or routing mechanism responsible for the non-monotonic pattern.

None of the three initial-storage settings produced peak enhancement in the six events. Some settings produced zero attenuation, so the observed response range includes both unchanged and reduced peak magnitudes.

4.3.5 Sensitivity to the spill-threshold coefficient

At a fixed initial storage ratio of 0.50, peak-attenuation ranges across S5, S4 and S2 were 0.99-1.20%, 0-1.27%, 0.69-1.86%, −0.22-2.04%, 0-0.63% and 1.12-1.33%, respectively (Figure 6b). Event 230528 had the largest range, exceeding two percentage points.

Mean peak attenuation increased from 0.57% at a spill threshold of 0.85 to 0.65% at 0.90 and 1.27% at 0.95. Mean pre-peak flow reduction increased from 0.52% to 0.96% between the lowest and highest thresholds. Available storage before spilling increased from 0.35 to 0.45 times node capacity over this sequence.

Attenuation increased with the threshold in four events. Event 240711 showed the opposite pattern, changing from 0.63% to 0.24% and then to zero. Event 250929 was non-monotonic, with values of 1.33%, 1.12% and 1.27%. Event 230528 changed from slight enhancement (−0.22%) to attenuation (0.27% and 2.04%).

Only event 230528 changed the sign of its peak response within the tested threshold sequence. Explaining that change requires node release, storage and routing trajectories; outlet peak values alone cannot establish a flood-wave synchronization mechanism.

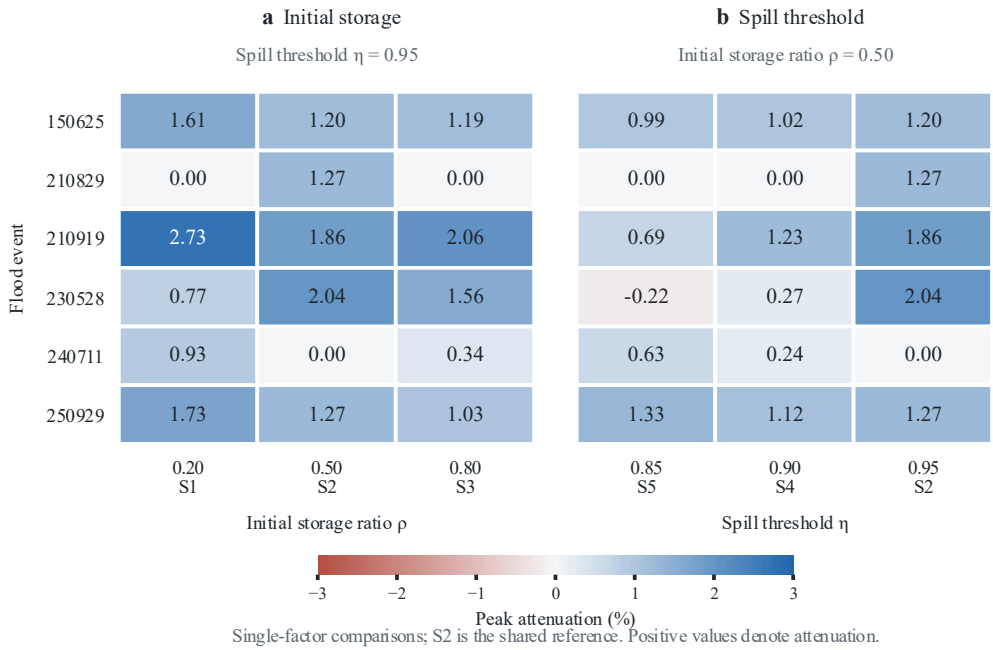


Figure 6. Peak-attenuation sensitivity to (a) initial storage ratio at a fixed spill threshold of 0.95 and (b) spill threshold at a fixed initial storage ratio of 0.50. Cell labels are percentages relative to BTOP; positive values denote attenuation and negative values enhancement. Both panels use the same zero-centred colour scale, and S2 is repeated as the common reference. These are one-factor-at-a-time comparisons, not a full factorial experiment.

4.3.6 Response ranges over the tested parameter intervals

Mean event-level peak-attenuation ranges were 0.91 percentage points across initial-storage ratios and 0.96 percentage points across spill thresholds. The first interval spans 0.20-0.80, whereas the second spans 0.85-0.95. Their similar response ranges therefore do not demonstrate equal intrinsic parameter importance. They also do not quantify interactions between the two parameters.

The reference scenario supports event comparisons under a common assumed state, while the two parameter sequences show how the reported response changes across selected settings. These ranges are conditional on the supplied forcing, calibrated BTOP structure and simplified node rules. They should not be presented as probabilistic uncertainty limits or exhaustive bounds on small-reservoir regulation.

5. Discussion

5.1 Contribution and evidence for distributed representation

The storage-balance equation and threshold-release concept are established modelling components. Relative to the reference BTOP implementation, the present addition is their placement at tributary nodes and the replacement of controlled inflow by regulated outflow before downstream routing. Existing distributed reservoir models and coupling alternatives provide relevant precedents[34]. The present contribution is therefore an implementation and case-specific assessment under limited operating data, rather than the invention of distributed reservoir modelling.

The current experiments establish differences between BTOP with and without the specified nine-node module. They do not isolate the value of node distribution or validate the 15-to-nine aggregation. That requires matched comparisons with a single aggregate and an individual-reservoir representation. Such comparisons should conserve total capacity, surface area, initial storage and the intercepted runoff volume, and should keep release assumptions and BTOP parameters fixed. A reservoir placed at the outlet must not intercept additional basin runoff simply because of its location. Otherwise, changes attributed to spatial representation would also include differences in controlled drainage area.

5.2 Interpreting the small outlet signal

The inventoried nominal storage of 2,919,530 m^3 is equivalent to about 1.36 mm spread over the 2,146.8 km^2 basin. Under S2, storage available before spilling is 45% of that total, or 1,313,788.5 m^3, equivalent to about 0.61 mm over the basin. These values place the inventory in basin-scale context and are consistent with investigating a small outlet signal. They are not bounds on peak attenuation: the response also depends on the intercepted runoff, event volume and timing, and bypass flow.

A small simulated effect is informative when its size and conditions are reported transparently. Here, it limits the support for assuming a substantial basin-wide benefit from this reservoir inventory during the six selected events. It does not exclude larger

local effects on individual tributaries, which were not quantified by the outlet metrics, or larger effects in basins with different storage and connectivity. Because actual reservoir states were unobserved, the estimated percentages should not be treated as measured flood-control benefits or directly prescribed as operational reduction factors.

5.3 Parameter dependence and unresolved process interpretation

Initial storage and the spill threshold both affect storage available before spilling, as shown in Equ.16. They therefore have partly over lapping roles in this simplified rule. The separate parameter sequences reveal conditional response ranges but cannot identify joint effects or establish which parameter is intrinsically more influential. A full factorial experiment, together with checks on when storage becomes empty or reaches the threshold, would be required to examine that dependence more fully.

The non-monotonic responses in several exported event series require particular care. For a fixed inflow, capacity, spill threshold and background-release rule, the stated node update imposes an ordering on releases as initial storage changes. A non-monotonic outlet response therefore requires examination of the full coupling and routing implementation before it is attributed to tributary-wave synchronization. Node inflow, bypass flow, release, storage and downstream routing trajectories should be compared at matching time steps, together with scenario configuration and export provenance. The present outlet statistics do not complete that process verification.

5.4 Scope and remaining validation needs

Several limitations constrain transfer. The six events were selected for large observed peaks and complete records, rather than as a random flood sample. The observed flow used to calibrate BTOP may already incorporate reservoir influences, so the reference configuration is not an independently observed natural baseline. The node rule omits individual operating decisions and continuous level-dependent release behaviour, and uses simulated low flow as a background-release proxy. Aggregating reservoirs removes within-tributary travel times and variations in storage state. The single-event water-balance check establishes closure only for that reported calculation.

Rainfall, reservoir capacity, background release, catchment parameters and structural uncertainty were not jointly propagated. Process checks across all scenarios, matched comparisons of one, nine and 15 reservoir nodes, and independent level or release observations would provide stronger tests than outlet scenario differences alone. Cross-basin evaluation is also needed before inferring applicability to denser reservoir networks or other hydroclimatic conditions.

6. Conclusions

BTOP-DRN adds tributary storage-release calculations to a fixed BTOP configuration and represents 15 reservoirs as nine equivalent nodes. The contribution is an explicit scenario-based assessment of event-scale regulation under limited operating data. The experiments compare this implementation with BTOP without explicit nodes; they do not establish that nine nodes outperform a single aggregate or individual-reservoir representation.

The BTOP parameter set transferred consistently to six independent events, with NSE values of 0.74-0.87 and a mean of 0.81. The reservoir-node module closed the water balance to $4.08 \times 10{-}6\%$ in the representative test and respected storage constraints. These checks support numerical consistency, but not validation of historical reservoir operation. BTOP-DRN remains a conceptual, scenario-based representation because reservoir-level observations were unavailable.

Under the reference state, simulated outlet peak attenuation ranged from 0 to 2.04% and averaged 1.27%. Mean pre-peak discharge reduction ranged from 0 to 2.03%, and event-volume reduction ranged from −0.18% to 0.49%. Outlet peak time changed by at most one hourly step, without a systematic delay. These values characterize the six analysed Qianhe events and the prescribed reservoir state.

Peak response varied across the tested storage and threshold settings, including a change from −0.22% to 2.04% in event 230528. Similar mean response ranges over the two parameter intervals do not establish equal parameter importance, and non-monotonic outlet patterns require further process verification. The practical implication

is to report conditional event-specific effects rather than applying a fixed basin-wide reduction factor. Wider transfer requires structural comparisons and independent constraints on reservoir storage and releases.

Authors Contributions

For this research paper with several authors, a short paragraph specifying their individual contributions was provided. Zehua Lu and Ming Li developed the original idea and contributed to the research design for the study. ZeHua Lu was responsible for data collecting. Tianqi Ao, and Liwen Xing provided guidance and improving suggestion. Tianqi Ao, and Liwen Xing some guidance for the writing of the article. Zehua Lu provided ideas for the mapping in this paper. All authors have read and approved the final manuscript.

Funding

This research received no external funding.

Declaration of competing interest

The authors declare that there is no conflict of interest regarding the publication of this paper.

Availability of data and material

The public datasets that support the findings of this study are specified with their access addresses in the article. The rainfall and runoff data are available from the Changjiang River Scientific Research Institute (CRSRI), but restrictions apply to the availability of these data, which were used under license for the current study, and so are not publicly available. Data are however available from the authors upon reasonable request and with permission of the Changjiang River Scientific Research Institute (CRSRI). The rainfall and runoff datasets analysed during the current study are not

publicly available but are available from the corresponding author on reasonable request.

References

1 Westra, S. *et al.* Future changes to the intensity and frequency of short-duration extreme rainfall. *REVIEWS OF GEOPHYSICS* **52**, 522-555, doi:10.1002/2014RG000464 (2014).

2 Prein, A. F. *et al.* The future intensification of hourly precipitation extremes. *Nature Climate Change* **7**, 48-52, doi:10.1038/nclimate3168 (2017).

3 Fowler, H. J. *et al.* Anthropogenic intensification of short-duration rainfall extremes. *Nature Reviews Earth & Environment* **2**, 107-122, doi:10.1038/s43017-020-00128-6 (2021).

4 Miao, Q., Yang, D., Yang, H. & Li, Z. Establishing a rainfall threshold for flash flood warnings in China's mountainous areas based on a distributed hydrological model. *JOURNAL OF HYDROLOGY* **541**, 371-386, doi:10.1016/j.jhydrol.2016.04.054 (2016).

5 Beven, K. J., Kirkby, M. J., Freer, J. E. & Lamb, R. A history of TOPMODEL. *HYDROLOGY AND EARTH SYSTEM SCIENCES* **25**, 527-549, doi:10.5194/hess-25-527-2021 (2021).

6 Gou, J. *et al.* Sensitivity Analysis-Based Automatic Parameter Calibration of the VIC Model for Streamflow Simulations Over China. *WATER RESOURCES RESEARCH* **56**, doi:10.1029/2019WR025968 (2020).

7 Golmohammadi, G., Prasher, S., Madani, A. & Rudra, R. Evaluating Three Hydrological Distributed Watershed Models: MIKE-SHE, APEX, SWAT. *Hydrology* **1**, 20-39 (2014).

8 Sivapalan, M. *et al.* IAHS decade on Predictions in Ungauged Basins (PUB), 2003-2012: Shaping an exciting future for the hydrological sciences. *HYDROLOGICAL SCIENCES JOURNAL-JOURNAL DES SCIENCES HYDROLOGIQUES* **48**, 857-880, doi:10.1623/hysj.48.6.857.51421 (2003).

9 Takeuchi, K., Ao, T. Q. & Ishidaira, H. Introduction of block-wise use of TOPMODEL and Muskingum-Cunge method for the hydro-environmental simulation of a large ungauged basin. *HYDROLOGICAL SCIENCES JOURNAL-JOURNAL DES SCIENCES HYDROLOGIQUES* **44**, 633-646, doi:10.1080/02626669909492258 (1999).

10 Bao, H.-j., Wang, L.-l., Li, Z.-j., Zhao, L.-n. & Zhang, G.-p. Hydrological daily rainfall-runoff simulation with BTOPMC model and comparison with Xin'anjiang model. *Water Science and Engineering* **3**, 121-131, doi:https://doi.org/10.3882/j.issn.1674-2370.2010.02.001 (2010).

11 Zhu, Y. *et al.* Application of the Regression-Augmented Regionalization Approach for BTOP Model in Ungauged Basins. *Water* **13**, doi:10.3390/w13162294 (2021).

12 Nimai, S. *et al.* Enhancing Runoff Simulation Using BTOP-LSTM Hybrid Model in the Shinano River Basin. *Water* **15**, doi:10.3390/w15213758 (2023).
13 Zhou, L. & Liu, L. Enhancing dynamic flood risk assessment and zoning using a coupled hydrological-hydrodynamic model and spatiotemporal information weighting method. *Journal of Environmental Management* **366**, doi:10.1016/j.jenvman.2024.121831 (2024).
14 Nilsson, C., Reidy, C. A., Dynesius, M. & Revenga, C. Fragmentation and Flow Regulation of the World's Large River Systems. *Science* **308**, 405-408, doi:10.1126/science.1107887 (2005).
15 Poff, N. L., Olden, J. D., Merritt, D. M. & Pepin, D. M. Homogenization of regional river dynamics by dams and global biodiversity implications. *Proceedings of the National Academy of Sciences* **104**, 5732-5737, doi:10.1073/pnas.0609812104 (2007).
16 Habets, F., Molénat, J., Carluer, N., Douez, O. & Leenhardt, D. The cumulative impacts of small reservoirs on hydrology: A review. *Science of The Total Environment* **643**, 850-867, doi:https://doi.org/10.1016/j.scitotenv.2018.06.188 (2018).
17 Habets, F., Philippe, E., Martin, E., David, C. H. & Leseur, F. Small farm dams: impact on river flows and sustainability in a context of climate change. *Hydrol. Earth Syst. Sci.* **18**, 4207-4222, doi:10.5194/hess-18-4207-2014 (2014).
18 Rabelo, U. P. *et al.* Impact of Dense Networks of Reservoirs on Streamflows at Dryland Catchments. *Sustainability* **14**, 14117 (2022).
19 Peter, S. J., de Araújo, J. C., Araújo, N. A. M. & Herrmann, H. J. Flood avalanches in a semiarid basin with a dense reservoir network. *Journal of Hydrology* **512**, 408-420, doi:https://doi.org/10.1016/j.jhydrol.2014.03.001 (2014).
20 Lebon, N., Dagès, C., Burger-Leenhardt, D. & Molénat, J. A new agro-hydrological catchment model to assess the cumulative impact of small reservoirs. *Environmental Modelling & Software* **153**, 105409, doi:https://doi.org/10.1016/j.envsoft.2022.105409 (2022).
21 Evin, G. *et al.* Evaluation of hydrological models on small mountainous catchments: impact of the meteorological forcings. *Hydrol. Earth Syst. Sci.* **28**, 261-281, doi:10.5194/hess-28-261-2024 (2024).
22 Ding, W., Wei, G. & Zhou, H. Improving flood resilience through optimal reservoir operation. *Journal of Hydrology* **620**, 129494, doi:https://doi.org/10.1016/j.jhydrol.2023.129494 (2023).
23 Yan, X. *et al.* Impacts of small and medium-sized reservoirs on streamflow in two basins of Southeast China, using a hydrological model to separate influences of multiple drivers. *Journal of Hydrology: Regional Studies* **50**, 101582, doi:https://doi.org/10.1016/j.ejrh.2023.101582 (2023).
24 Colombo, P., Ribeiro Neto, G. G., Costa, A. C., Mamede, G. L. & Van Oel, P. R. Modeling the influence of small reservoirs on hydrological drought

propagation in space and time. *Journal of Hydrology* **629**, 130640, doi:https://doi.org/10.1016/j.jhydrol.2024.130640 (2024).

25 Shrestha, P. K. *et al.* Toward Improved Simulations of Disruptive Reservoirs in Global Hydrological Modeling. *Water Resources Research* **60**, doi:10.1029/2023wr035433 (2024).

26 Dong, N. *et al.* Model Estimates of China's Terrestrial Water Storage Variation Due To Reservoir Operation. *Water Resources Research* **58**, e2021WR031787, doi:https://doi.org/10.1029/2021WR031787 (2022).

27 Borga, M., Anagnostou, E. N., Bloschl, G. & Creutin, J. D. Flash floods Observations and analysis of hydro-meteorological controls Preface. *JOURNAL OF HYDROLOGY* **394**, 1-3, doi:10.1016/j.jhydrol.2010.07.048 (2010).

28 Muñoz-Sabater, J. *et al.* ERA5-Land: a state-of-the-art global reanalysis dataset for land applications. *Earth Syst. Sci. Data* **13**, 4349-4383, doi:10.5194/essd-13-4349-2021 (2021).

29 Marra, F., Koukoula, M., Canale, A. & Peleg, N. Predicting extreme sub-hourly precipitation intensification based on temperature shifts. *Hydrol. Earth Syst. Sci.* **28**, 375-389, doi:10.5194/hess-28-375-2024 (2024).

30 Knoben, W. J. M., Freer, J. E. & Woods, R. A. Technical note: Inherent benchmark or not? Comparing Nash–Sutcliffe and Kling–Gupta efficiency scores. *Hydrol. Earth Syst. Sci.* **23**, 4323-4331, doi:10.5194/hess-23-4323-2019 (2019).

31 Zhang, X. *et al.* GLC_FCS30: global land-cover product with fine classification system at 30 m using time-series Landsat imagery. *Earth Syst. Sci. Data* **13**, 2753-2776, doi:10.5194/essd-13-2753-2021 (2021).

32 Hosseini-Moghari, S. M. & Döll, P. The value of observed reservoir storage anomalies for improving the simulation of reservoir dynamics in large-scale hydrological models. *Hydrol. Earth Syst. Sci.* **29**, 4073-4092, doi:10.5194/hess-29-4073-2025 (2025).

33 Steyaert, J. C., Sutanudjaja, E. H., Bierkens, M. & Wanders, N. Data derived reservoir operations simulated in a global hydrologic model. *Hydrol. Earth Syst. Sci.* **29**, 6499-6527, doi:10.5194/hess-29-6499-2025 (2025).

34 Vora, A., Cai, X., Chen, Y. & Li, D. Coupling Reservoir Operation and Rainfall-Runoff Processes for Streamflow Simulation in Watersheds. *Water Resources Research* **60**, e2023WR035703, doi:https://doi.org/10.1029/2023WR035703 (2024).